Supported Liquid-Phase Catalytic Membrane Reactor-Separator for Homogeneous Catalysis

Jae S. Kim and Ravindra Datta
Dept. of Chemical and Biochemical Engineering, University of Iowa, Iowa City, IA 52242

A new configuration of a membrane reactor-separator for homogeneous catalysis is described that is designed not only to encapsulate the catalyst solution, but to simultaneously separate the product from reactant. It is composed of a porous support layer that is impregnated partially or completely with the liquid-phase catalyst and is sandwiched between two different membranes. Membrane 1 is readily permeable to the reactant but not to the product, whereas membrane 2 allows free permeation of both the reactant and the product while encapsulating the catalyst solution. The performance of a differential stirred-cell membrane reactor-separator was theoretically investigated for the case of a first-order irreversible reaction. The extent of product separation was studied as a function of membrane permselectivity for reactant and product, the difference in resistance of membrane and catalyst layer, liquid loading of the catalyst layer, and the sweep fluid flow rate. The efficacy of the device was experimentally demonstrated using ethylene hydroformylation with hydridocarbonyltris (triphenyl phosphine) Rh(I) catalyst dissolved in dioctyl phthalate solvent.

Introduction

Although the vast majority of the industrial catalytic processes involve heterogeneous catalysts, there are now many industrial processes that utilize homogeneous catalysts (Parshall, 1978, 1981; Parshall and Putscher, 1986). The chief advantages of homogeneous catalysis are the high selectivity, relatively mild reaction conditions, molecular dispersion of the catalyst, and controllability of the nature of the catalytically active species. However, there are also some disadvantages such as the required separation from the product and recycle of the catalyst, the attendant corrosion and catalyst losses, and ineffective catalyst utilization for reactions involving a gaseous reactant due to the relatively low gas-liquid interfacial area obtainable in conventional gas-sparged reactors.

Different hybrid techniques (Hartley, 1985) have, therefore, been developed in an effort to overcome some of these problems and to combine the attractive features of homogeneous catalysis with those of heterogeneous catalysis, like convenient handling, large interfacial area, and ease of separation of the catalyst and reaction mixture. These include: i) supported liquid-phase catalysis (SLPC) (Rony, 1968; Rony and Roth, 1975; Datta and Rinker, 1985), in which the liquid-phase catalyst is coated on the pore walls of a porous support; ii) supported molten-salt catalysis (SMSC) (Rao and Datta, 1988) which avoids solvent volatilization encountered in SLPC; iii) matrix-bound complexes (Murrell, 1977; Pittman, 1982; Hartley, 1985); iv) zeolite-entrapped complexes (Davis et al., 1986); and v) catalytic liquid membrane (Ollis et al., 1972).

In this article, we describe a novel supported liquid-phase catalytic membrane reactor-separator (SLPCMRS) for homogeneous catalysis that is designed not only to immobilize the catalyst solution as done in the SLPC technique, but to simultaneously effect continuous separation of reactants and products in a single device (Kim and Datta, 1987). Membrane reactors, which contain immobilized membrane-bound or encapsulated enzymes or cells, have been extensively studied for biocatalyzed reactions (Cheryan, 1986; Cheryan and Mehaia, 1986). Membrane reactors utilizing inorganic membranes have also recently been investigated for heterogeneous catalysis. However, this is the first such study involving homogeneous catalysis (Haggin, 1988).

The membrane reactors for biocatalysis exploit the large size difference between the biocatalyst, enzymes or cells, and the substrate and the product. Thus, the biocatalyst is easily retained by the semipermeable membrane which allows free passage of the reacting substrate and products. Rony (1971, 1972)

Correspondence concerning this article should be addressed to R. Datta.

proposed encapsulation of enzyme solution by drawing it by capillary action into small-diameter hollow fibers and sealing the ends. He also developed a mathematical model for diffusion and reaction in membrane encapsulated enzyme solution. The feasibility of the concept was experimentally demonstrated in a batch system containing a bundle of loaded hollow fibers, which allowed the passage of both substrate and product but effectively retained the enzyme (Davis, 1974). Vick Roy et al. (1983), on the other hand, encapsulated the biocatalyst on the shell side of the hollow-fiber module. Wang et al. (1970) used an ultrafiltration unit in series with a continuous stirred-tank bioreactor. Others (for example, Hong et al., 1981) have combined the two units by incorporating an ultrafiltration membrane within a pressurized stirred-tank bioreactor.

Matson and Quinn (1986) proposed a novel membrane reactor-separator for enzyme-catalyzed reactions that combines reaction, separation, and product enrichment in a single process. The SLPCMRS described here is an extension of this approach for application to homogeneous catalysis. The reactor-separator developed by Matson and Quinn consists of a bilayer of a permselective membrane through which the substrate permeates and encounters a second membrane containing the immobilized enzyme, where it undergoes reaction to form the product. The concept was demonstrated for the chymotrypsin-catalyzed, stereoselective hydrolysis of *N*-acetyl-*L*-tyrosine ethyl ester. The permselective membrane, prepared by impregnating a microporous Teflon membrane with water immiscible l-decanol, possessed low permeability for the ionized product, and hence, the product was forced to diffuse to the opposite side where it was collected with a sweep fluid. The device not only effectively separated the substrate and product, but also simultaneously concentrated the product to a concentration substantially higher than that of the substrate in feed at high feed-to-product stream flow rate ratios.

While the literature on the utilization of membrane reactors for biocatalysis is substantial (Cheryan, 1986), little effort seems to have been devoted to extending these techniques for application to homogeneous catalysis. Jennings and Binning (1960) used water-permeable membrane to eliminate water produced in the reaction of *n*-butanol and acetic acid and thus drive the reaction to completion. Gosser et al. (1973, 1977) used reverse osmosis cells to obtain good separation of several soluble transition metal complexes from reaction mixtures after completion of reaction.

Membrane reactors with inorganic membranes recently have also been utilized for heterogeneous catalysis. Shinji et al. (1982) studied cyclohexane dehydrogenation to benzene in a double-tubular membrane reactor consisting of a packed bed of Pt/Al_2O_3 in a microporous vycor glass tube enclosed within a nonporous tube. Enhanced conversion was obtained due to the selective diffusion of one of the reaction products, H_2, through the vycor glass. Itoh (1987) also studied cyclohexane dehydrogenation in a packed-bed membrane reactor but used a thin (25-μm) palladium tubular membrane. Due to the highly selective diffusion of H_2 through the palladium membrane, almost complete conversion was achieved at low space velocities as compared with the equilibrium conversion of only 18.7% at the reaction temperature of 473 K. Sun and Khang (1988) also obtained enhanced conversion of cyclohexane in a membrane reactor consisting of a porous vycor glass membrane with Pt catalyst deposited on it.

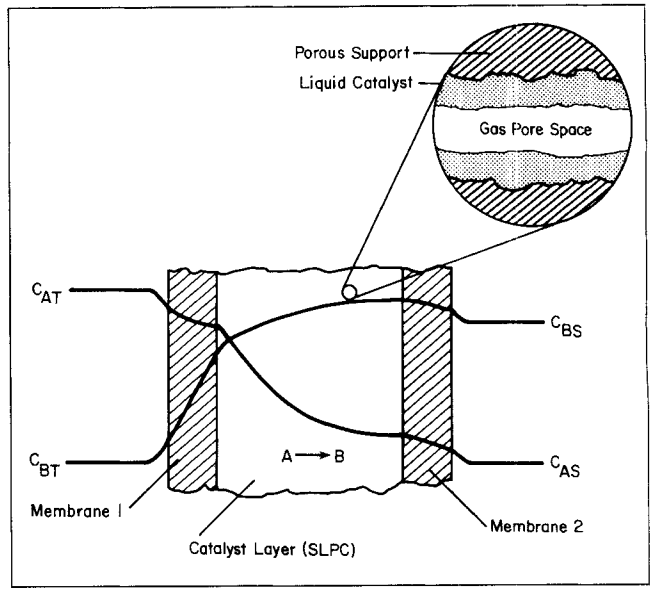

Figure 1. Membrane-catalyst-membrane composite in SLPCMRS.

Supported Liquid-Phase Catalytic Membrane Reactor-Separator

The concept of the supported liquid-phase catalytic membrane reactor-separator is explained in Figure 1. The SLPCMRS consists of a porous matrix supported liquid-phase catalyst (SLPC) layer sandwiched between two different membranes. The catalyst-membrane composite is contacted on the left side with the feed stream consisting of reactant A. Membrane 1 is chosen to be relatively freely permeable to the reactant but to provide a significant permeability barrier to product B. For this discussion, it is assumed that the reactant undergoes an irreversible catalytic reaction, $A \rightarrow B$, in the SLPC layer to form the product. If both the reactant and the product are in a gaseous or vaporous form, it is advantageous to only partially impregnate the porous support with the catalyst solution (Rony, 1968; Datta and Rinker, 1985). At low liquid catalyst loading q, defined as the fraction of the pore volume of the support that is occupied by the catalyst solution, the reaction rate increases with q, but goes through a maximum at an intermediate value of q, finally reducing at higher values of q due to the increased diffusional resistance in the SLPC layer. If, however, the reactant and/or the product are in the liquid phase, $q = 1$ is appropriate. In any case, the concentration of A drops off in the SLPC layer due to diffusional resistance, while that of B increases. If the SLPC layer is sufficiently thick, reactant A may be completely exhausted toward the product side for an irreversible reaction. Membrane 2 may, thus, be chosen to be freely permeable to both the reactant and the product, its main function being the encapsulation of the catalyst solution. Since the permeability of the product in membrane 2 is much higher than that in membrane 1, the product predominantly diffuses to the right where it is collected in the product chamber with or without the help of a sweep fluid. The SLPCMRS configuration shown in Figure 1 provides the following benefits:

- It encapsulates the liquid-phase catalyst solution, thus obviating the separation of catalyst from the product.

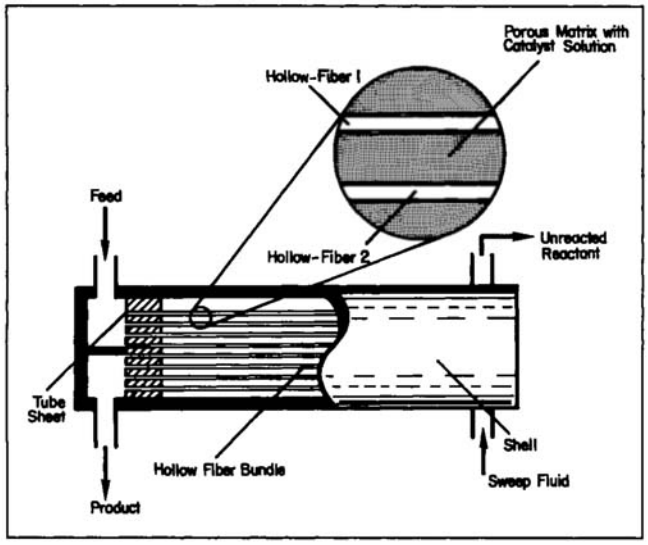

Figure 2. Shell-and-tube configuration for SLPCMRS utilizing two different hollow-fiber membranes.

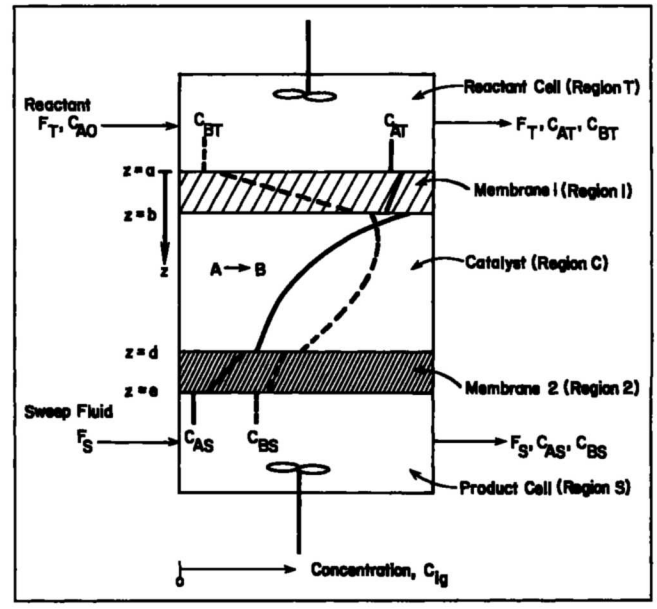

Figure 3. Membrane-catalyst-membrane composite in a stirred-cell reactor-separator.

- It can eliminate or substantially reduce the corrosion encountered in many conventional homogeneous catalytic processes by immobilizing the catalyst solution.
- It separates the product from the reactant, thus eliminating or reducing the conventional separation steps.
- It can provide product *enrichment* if the product stream flow rate is sufficiently small as compared with the reactant-feed flow rate.
- It can provide more effective catalyst utilization for reaction systems involving a gaseous reactant or product by providing a substantially higher gas-liquid interfacial area in the SLPC layer than is possible in conventional gas-sparged liquid-phase reactors. This is a significant advantage since many reactions, such as hydrogenation, oxidation, carbonylation, and hydroformylation, involve a gaseous reactant.
- It can facilitate contact in multiphase reaction systems, for example, those involving species soluble in aqueous and organic phases (Matson and Quinn, 1986).
- It can steer reaction pathways or provide higher conversions in reactions with unfavorable reaction equilibrium by simultaneous removal of the product or by selective removal or entrapment of one of the species (Matson and Quinn, 1986).

For practical applications, use of hollow fibers should provide large interfacial areas. As shown in Figure 2, a possible design could be a shell-and-tube configuration consisting of two different hollow fibers corresponding to membranes 1 and 2. The catalyst solution is supported on a porous matrix on the shell side. Thus, the feed mixture is introduced on the tube side and flows through hollow fibers corresponding to membrane 1. It diffuses through the fiber wall to the shell side and undergoes reaction in the SLPC region. The product, being largely impermeable in hollow fiber 1, diffuses preferentially through hollow fiber 2, where it may be collected with or without the help of a sweep fluid. Further, cocurrent and countercurrent flow configurations are possible.

Theoretical Analysis

Although integral reactor-separators, such as shown in Figure 2, are of interest for actual applications, the concept is demonstrated here by investigating a differential reactor-separator. Figure 3 shows the cross-section of the catalyst membrane composite placed in a stirred cell. The composite consists of a porous layer of thickness L_C impregnated with the catalyst solution and sandwiched between two different membranes. Feed is introduced into the top (reactant) cell at a constant volumetric flow rate F_T and a reactant concentration C_{AO}. Reactant A permeates through membrane 1 and undergoes an irreversible, homogeneous catalytic reaction to form product B in the catalyst layer. The product preferentially diffuses toward the lower compartment and permeates out through membrane 2 along with any unconverted reactant. A sweep fluid with a constant volumetric flow rate F_S in the lower (product) cell removes the product and any unconverted reactant. The steady-state conservation equations for species A and B in the different regions shown in Figure 3 are:

Region T:

$$F_T(C_{i0} - C_{iT}) = N_{i2}(a) \cdot A \tag{1}$$

Region 1:

$$D_{i1}\frac{d^2C_{i1}}{dz^2} = 0 \tag{2}$$

Region C:

$$D_{iC}\frac{d^2C_{iC}}{dz^2} + R_i = 0 \tag{3}$$

Region 2:

$$D_{i2}\frac{d^2C_{i2}}{dz^2} = 0 \tag{4}$$

Region S:

$$F_S C_{iS} = N_{iz}(e) \cdot A \tag{5}$$

where the subscript *ig* refers to a quantity associated with species *i* (*A* or *B*) in region *g*. Equations 2 and 4 are based on the assumption of a Fickian membrane transport model, both for dense membranes, in which the solution-diffusion model is usually employed, as well as for microporous membranes, in which the transport is predominantly by Knudsen diffusion. In Eq. 5, it is assumed that the sweep fluid inlet to the lower cell contains no reactant or product. The effective diffusivity in the catalyst region is given (Datta and Rinker, 1985) by:

$$D_{iC} = \frac{(1-q)^2}{K_{iL}} D_{ije} + q^2 D_{iL} \tag{6}$$

where D_{ije} and D_{iL} are the effective binary gas-phase diffusivity and liquid-phase diffusivity, respectively. Equation 6 accounts for the simultaneous transport of species *i* in the residual gas pore space, as well as the liquid phase, and is based on the assumption that tortuosity factor = 1/porosity, as given by the random pore model.

For negligible fluid-phase boundary-layer resistance on either side of the composite, solution to Eqs. 2 and 4 for appropriate boundary conditions gives:

$$N_{iz}(a) = P_{i1}\left\{C_{iT} - \frac{C_{iC}(b)}{K_{iC}}\right\} = N_{iz}(b) \tag{7}$$

and

$$N_{iz}(d) = P_{i2}\left\{\frac{C_{iC}(d)}{K_{iC}} - C_{iS}\right\} = N_{iz}(e) \tag{8}$$

where the permeabilities for the two membranes are defined by $P_{i1} \equiv D_{i1} K_{i1}/L_1$ and $P_{i2} \equiv D_{i2} K_{i2}/L_2$. Here, K_{i1} and K_{i2} are the partition coefficients of species *i* in membranes 1 and 2, respectively. Equation 3 is subject to the following boundary conditions:

At $z = b$:

$$C_{iC} = C_{iC}(b) \tag{9}$$

and

$$N_{iz}(b) = P_{i1}\left\{C_{iT} - \frac{C_{iC}(b)}{K_{iC}}\right\} = -D_{iC}\frac{dC_{iC}(b)}{dz} \tag{10}$$

At $z = d$:

$$C_{iC} = C_{iC}(d) \tag{11}$$

and

$$N_{iz}(d) = P_{i2}\left\{\frac{C_{iC}(d)}{K_{iC}} - C_{iS}\right\} = -D_{iC}\frac{dC_{iC}(d)}{dz} \tag{12}$$

For reactant *A*, Eq. 3 takes the following form for a first-order irreversible reaction, $A \xrightarrow{k} B$:

$$D_{AC}\frac{d^2 C_{AC}}{dz^2} - \epsilon q k C_{AC} = 0 \tag{13}$$

The solution to Eq. 13 subject to Eqs. 9 and 11 in terms of the concentrations at the catalyst layer boundaries is:

$$C_{AC} = C_{AC}(b)\frac{\sinh[\phi(1-y)]}{\sinh\phi} + C_{AC}(d)\frac{\sinh(\phi y)}{\sinh\phi} \tag{14}$$

where the dimensionless distance in the SLPC layer, $y \equiv (z-b)/L_C$, and the Thiele modulus for the SLPC layer:

$$\phi \equiv L_C\sqrt{\frac{\epsilon q k}{D_{AC}}} \tag{15}$$

Next, Eq. 14 is used in Eqs. 10 and 12 to obtain the interfacial concentrations, $C_{AC}(b)$ and $C_{AC}(d)$, in terms of the reactant concentration in the reactant and product cells, C_{AT} and C_{AS}, respectively:

$$\frac{C_{AC}(b)}{K_{AC}} = \frac{C_{AT}(1 + \Lambda_2\phi\coth\phi) + C_{AS}\Lambda_1\dfrac{\phi}{\sinh\phi}}{1 + (\Lambda_1 + \Lambda_2)\phi\coth\phi + \Lambda_1\Lambda_2\phi^2} \tag{16}$$

and

$$\frac{C_{AC}(d)}{K_{AC}} = \frac{C_{AS}(1 + \Lambda_1\phi\coth\phi) + C_{AT}\Lambda_2\dfrac{\phi}{\sinh\phi}}{1 + (\Lambda_1 + \Lambda_2)\phi\coth\phi + \Lambda_1\Lambda_2\phi^2} \tag{17}$$

where the relative membrane resistances or permeability ratios, $\Lambda_1 \equiv P_{AC}/P_{A1}$ and $\Lambda_2 \equiv P_{AC}/P_{A2}$. In these, a permeability for the catalyst layer is defined, in analogy to that for membranes, by $P_{AC} \equiv D_{AC} K_{AC}/L_C$. Substitution of Eqs. 16 and 17 back into Eq. 14 gives the reactant concentration profile in the catalyst layer in terms of C_{AT} and C_{AS}. The concentration profile within the membranes are, of course, linear.

The fluxes of the reactant into the composite in the upper compartment and out of the composite in the lower compartment are given by Eqs. 7 and 8 and also by Eqs. 1 and 5. Thus,

$$N_{Az}(a) = P_{A1}\left\{C_{AT} - \frac{C_{AC}(b)}{K_{AC}}\right\} = \frac{F_T}{A}(C_{AO} - C_{AT}) \tag{18}$$

and

$$N_{Az}(e) = P_{A2}\left\{\frac{C_{AC}(d)}{K_{AC}} - C_{AS}\right\} = \frac{F_S}{A}C_{AS} \tag{19}$$

Substitution of Eqs. 16 and 17 into the above equations results in two expressions that may be solved simultaneously to obtain explicit expressions for C_{AT} and C_{AS} in terms of C_{AO}, and the dimensionless parameters, Λ_1, Λ_2, ϕ, and M_{AT} and M_{AS} defined by $M_{AT} \equiv F_T/AP_{AC}$ and $M_{AS} \equiv F_S/AP_{AC}$. Writing Eq. 3 for product *B* for a first-order irreversible reaction and adding

it to Eq. 13 and introducing y:

$$\frac{d^2C_{BC}}{dy^2} = -\Psi\frac{d^2C_{AC}}{dy^2} \tag{20}$$

where the diffusivity ratio, $\Psi \equiv D_{AC}/D_{BC}$. Integrating twice:

$$C_{BC} = -\Psi C_{AC} + a_1 y + a_2 \tag{21}$$

The constants of integration a_1 and a_2 are evaluated using Eqs. 9 and 11:

$$a_1 = [C_{BC}(d) - C_{BC}(b)] + \Psi[C_{AC}(d) - C_{AC}(b)] \tag{22}$$

and

$$a_2 = C_{BC}(b) + \Psi C_{AC}(b) \tag{23}$$

In the above equations, $C_{AC}(b)$ and $C_{AC}(d)$ are given by Eqs. 16 and 17. The interfacial concentrations for B are obtained using Eq. 21 in Eqs. 10 and 12. Differentiating Eq. 21 gives:

$$N_{Bz}(b) = -N_{Az}(b) - \frac{D_{BC}}{L_C}a_1 \tag{24}$$

and

$$N_{Bz}(d) = -N_{Az}(d) - \frac{D_{BC}}{L_C}a_1 \tag{25}$$

Using Eqs. 7, 8 and 22 in these equations:

$$P_{B1}\left\{C_{BT} - \frac{C_{BC}(b)}{K_{BC}}\right\} = -P_{A1}\left\{C_{AT} - \frac{C_{AC}(b)}{K_{AC}}\right\} - P_{BC}\left\{\frac{C_{BC}(d)}{K_{BC}} - \frac{C_{BC}(b)}{K_{BC}}\right\} - P_{AC}\left\{\frac{C_{AC}(d)}{K_{AC}} - \frac{C_{AC}(b)}{K_{AC}}\right\} \tag{26}$$

and

$$P_{B2}\left\{\frac{C_{BC}(d)}{K_{BC}} - C_{BS}\right\} = -P_{A2}\left\{\frac{C_{AC}(d)}{K_{AC}} - C_{AS}\right\} - P_{BC}\left\{\frac{C_{BC}(d)}{K_{BC}} - \frac{C_{BC}(b)}{K_{BC}}\right\} - P_{AC}\left\{\frac{C_{AC}(d)}{K_{AC}} - \frac{C_{AC}(b)}{K_{AC}}\right\} \tag{27}$$

Equations 26 and 27 can be solved simultaneously to provide the interfacial concentrations $C_{BC}(b)$ and $C_{BC}(d)$:

$$\frac{C_{BC}(b)}{K_{BC}} = \frac{(C_{BT} - \Lambda_3 X)(1 + \Lambda_4) + (C_{BS} + \Lambda_4 Y)\Lambda_3}{1 + \Lambda_3 + \Lambda_4} \tag{28}$$

and

$$\frac{C_{BC}(d)}{K_{BC}} = \frac{(C_{BT} - \Lambda_3 X)\Lambda_4 + (C_{BS} + \Lambda_4 Y)(1 + \Lambda_3)}{1 + \Lambda_3 + \Lambda_4} \tag{29}$$

where

$$X = \Psi\left[\left(1 - \frac{\phi}{\tanh\phi}\right)\frac{C_{AC}(b)}{K_{AC}} - \left(1 - \frac{\phi}{\sinh\phi}\right)\frac{C_{AC}(d)}{K_{AC}}\right] \tag{30}$$

and

$$Y = \Psi\left[\left(1 - \frac{\phi}{\sinh\phi}\right)\frac{C_{AC}(b)}{K_{AC}} - \left(1 - \frac{\phi}{\tanh\phi}\right)\frac{C_{AC}(d)}{K_{AC}}\right] \tag{31}$$

The permeability ratios, $\Lambda_3 \equiv P_{BC}/P_{B1}$, and $\Lambda_4 \equiv P_{BC}/P_{B2}$. Further, $P_{BC} \equiv D_{BC}K_{BC}/L_C$, and $C_{AC}(b)/K_{AC}$ and $C_{AC}(d)/K_{AC}$ are given by Eqs. 16 and 17.

The fluxes of product B are given by:

$$-N_{Bz}(a) = P_{B1}\left\{\frac{C_{BC}(b)}{K_{BC}} - C_{BT}\right\} = \frac{F_T}{A}C_{BT} \tag{32}$$

and

$$N_{Bz}(e) = P_{B2}\left\{\frac{C_{BC}(d)}{K_{BC}} - C_{BS}\right\} = \frac{F_S}{A}C_{BS} \tag{33}$$

Substitution of Eqs. 28 and 29 into the above equations results in C_{BT} and C_{BS} in terms of the dimensionless parameters, Λ_1, Λ_2, Λ_3, Λ_4, ϕ, and M_{BT} and M_{BS} defined by $M_{BT} \equiv F_T/AP_{BC}$ and $M_{BS} \equiv F_S/AP_{BC}$.

Finally, product separation is defined by:

$$\text{separation} \equiv \frac{N_{Bz}(e)}{N_{Bz}(e) - N_{Bz}(a)} = \frac{F_S/F_T}{F_S/F_T + C_{BT}/C_{BS}} \tag{34}$$

The second part of Eq. 34 results from the use of Eq. 32 for $N_{Bz}(a)$ and Eq. 33 for $N_{Bz}(e)$ with subsequent rearrangement, and is useful for the experimental evaluation of separation from the measurement of flow rates of reactant and product streams, F_T and F_S, and their product composition.

Experimental Apparatus and Methods

Reaction system

The hydroformylation of ethylene to form propionaldehyde catalyzed homogeneously by hydridocarbonyltris (triphenyl phosphine) Rh(I) was chosen as the model reaction system to demonstrate the feasibility of the SLPCMRS:

$$CH_2{=}CH_2 + H_2 + CO \rightarrow CH_3CH_2CHO \tag{35}$$

This reaction is chosen because it is relatively simple without any appreciable side products and is well studied (Parshall, 1981). Further, the reaction rate is rapid enough for appreciable conversion in a continuous-flow laboratory reactor under relatively mild conditions (Cornils, 1980), and the rate of reaction is pseudo-first order in ethylene concentration when hydrogen is in excess (Oliver and Booth, 1969).

Apparatus

A 400-mL stainless steel stirred cell (Nuclepore, model no. GH-400) was modified into a two-compartment membrane reactor-separator with provision for introducing and removing gases on either side of the catalyst-membrane composite. The

Table 1. Physical Properties of the Porous Support Disk

Parameter	Value
Material	Sintered stainless steel
Bulk density	4.94 g/cm^3
Diameter	76 mm
Thickness, L_C	5 mm
Porosity, ϵ	30.4%
Total surface area	450 cm^2
Average pore size	90 μm

Table 2. Properties of Membranes Used in SLPCMRS Experiments

Membrane	Supplier	Properties
1. UF Type F	Ultra/Por	Material: Cellulose Ester Hydrophobic MWCO: 10 K pH range: 1–14 Max. Temp.: 130°C Memb. Thickness*, $L_1 = 150$ μm Pore size**: 50 Å Porosity**: 1%
2. Filinert	Nuclepore	Material: PTFE Hydrophobic Porosity: 70–85% Bubble Point: 7–13 psi (48–90 kPa) Max. Temp.: 121°C Memb. Thickness*, $L_2 = 200$ μm Pore size**: 2,000 Å

*Determined by SEM.
**Determined from pure gas permeation experiments.

reactor was heated with an electric heating tape, and the temperature inside the reactor, measured by a platinum RTD sensor, was automatically controlled with a proportional temperature indicating controller (Cole Parmer, model no. 2155). The catalyst-membrane composite was placed between the upper and lower cells clamped together with a bracing ring. An O-ring placed above the composite provided the seal. The composite consisted of a porous stainless plate, with an average pore size of approximately 90 μm, impregnated with the catalyst solution and sandwiched between the two different membranes. The characteristics of the porous support disk and the two membranes used are provided in Tables 1 and 2, respectively.

The gases, hydrogen, carbon monoxide, and ethylene were purchased from Air Products and blended in the desired proportion by a high-pressure gas blending unit (Multiple Dyna-Blender, Matheson Model No. 8259). The gas mixture was fed to the reactor through a line pressure regulator for controlling the pressure in the reactor. Two three-way ball valves were used for bypassing the reactor for the chromatographic analysis of the feed mixture. A purge stream was fed to the lower compartment. The exit streams both from the top and bottom compartments were analyzed in an on-line HP5840A gas chromatograph equipped with an automatic gas sampling valve. A 1/8 in. × 6 ft. (3.2 mm × 1.8 m) Porapak-Q column was used with temperature programming from 50°C to 135°C at a rate of 20°C per minute. The GC was calibrated for all species. The exit tubing from the reactor to the gas chromatograph was wrapped with electric heating tape and maintained at 90°C to prevent any condensation of propionaldehyde in the lines. Exit stream gas flow rates were measured using soap bubble flowmeters. The experimental conditions used are summarized in Table 3.

Table 3. Experimental Conditions for Ethylene Hydroformylation in SLPCMRS

Parameter	Value
Reaction temperature	110°C
Reactant cell pressure	60–80 psi (410–550 kPa)
Product cell pressure	20–40 psi (140–280 kPa)
Liquid catalyst loading, q	0.1–0.5
Reactant stream flow rate, F_T	25 std. cm^3/min
Sweep stream (He) flow rate, F_S	0–100 std. cm^3/min
Catalyst	$RhH(CO)(PPh_3)_3$
Ligand	Triphenyl phosphine (PPh_3)
Solvent	Dioctylphthalate (b.p. = 384°C)
Rh concentration	5.3×10^{-3} mol/L
PPh_3/Rh molar ratio	50

SLP catalyst layer preparation

The catalyst, hydridocarbonyltris (triphenyl phosphine) Rh(I), and the ligand, triphenyl phosphine, were purchased from Strem Chemical Company. The catalyst solution was prepared by dissolving appropriate amounts of the catalyst and ligand in the solvent, dioctyl phthalate (DOP), purchased from Aldrich Company.

The catalyst, $RhHCO(PPh_3)_3$, the ligand, PPh_3, and the solvent, dioctyl phthalate were dissolved in acetone at room temperature. The mixture was magnetically stirred in a three-necked flask equipped with a total reflux condenser for several hours for complete dissolution. The volume ratio of DOP (normal boiling point = 384°C) and acetone (boiling point = 56.2°C) was determined based on the catalyst loading q desired (Datta et al., 1985). As an example, for $q = 0.1$, 10 vol. % DOP was added to 90 vol. % acetone, and then calculated amounts of the Rhodium catalyst and PPh_3 were dissolved in the DOP-acetone mixture. The porous disk was immersed in this solution and left overnight in a refrigerator to ensure complete penetration. Then, the disk was removed and the acetone evaporated by leaving the disk in fume hood for several hours. The actual liquid catalyst loading was checked by weight increase of the support disk.

Membranes utilized

As mentioned above, membrane 1 ideally should possess a high permeability for the reactant, but not for the product, whereas membrane 2 should allow free passage of both. Consequently, a nonporous membrane is indicated for membrane 1, while membrane 2 can be macroporous. However, it is difficult to find dense membranes that possess *both* a high permeability and a high permselectivity. On the other hand, microporous membranes provide high permeability, but low permselectivity. Thus, the selection of an appropriate membrane 1 may require a compromise between selectivity and permeability.

A number of different commercially available membranes were tested under reaction conditions. The chemical and thermal stability of the membranes was of paramount concern in the selection of the membranes. The characteristics of the membranes finally selected are listed in Table 2. Both of the

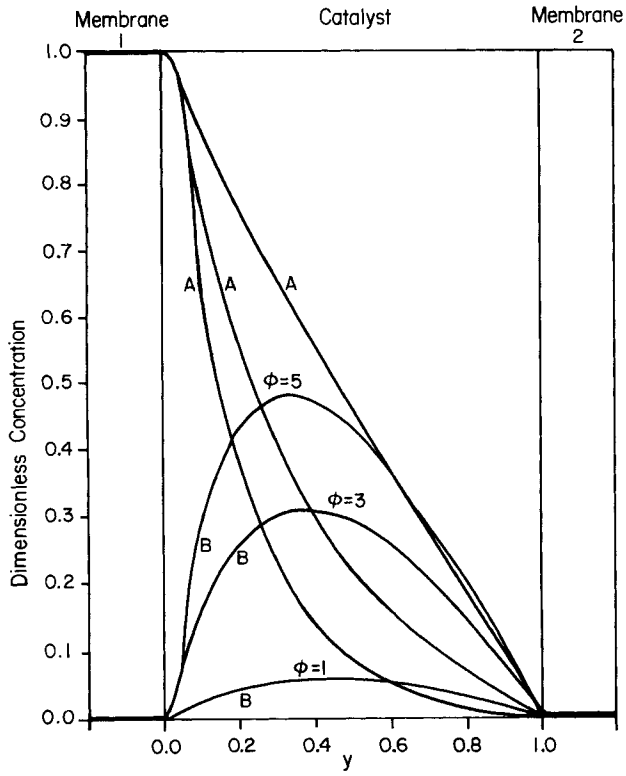

Figure 4. Dimensionless composition profiles of *A* and *B* in the composite at different values of Thiele modulus for the reaction *A*→*B*.

The membrane relative resistances are negligible (Λ_1 to $\Lambda_4 = 1 \times 10^{-4}$) and dimensionless reactant and product cell flow rates are very high (M_{iT}, $M_{iS} \to \infty$) so that $C_{AT}/C_T \to 1$, while C_{BT}/C_T, C_{AS}/C_T, and $C_{BS}/C_T \to 0$.

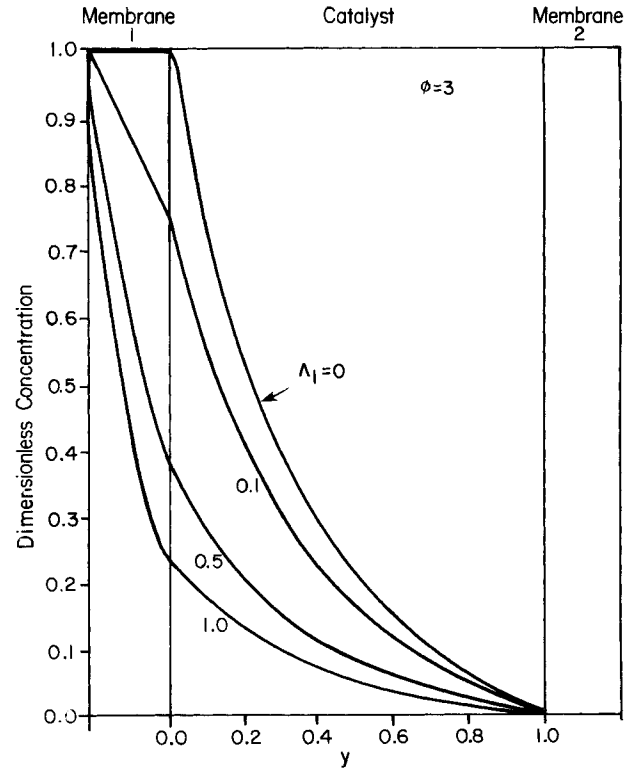

Figure 5. Effect of membrane 1 relative resistance (Λ_1) on the dimensionless reactant (*A*) concentration in the composite for $\phi = 3$ and negligible membrane 2 relative resistance, $\Lambda_2 = 1 \times 10^{-4}$.

The dimensionless reactant and product cell flow rates are very high (M_{iT}, $M_{iS} \to \infty$) so that $C_{AT}/C_T \to 1$, and $C_{AS}/C_T \to 0$.

membranes (PFTE and Cellulose Ester) are hydrophobic and, consequently, have limited interaction with the polar solvent, DOP. Further, both of the membranes chosen are microporous, but with very different values of pore size and porosity, because the low permeability of dense membranes was found to severely limit the conversion obtainable. This was at the expense of high permselectivity of reactant (ethylene) and product (propionaldehyde) in membrane 1, which under Knudsen diffusion control, was $P_{A1}/P_{B1} = \sqrt{M_B/M_A} = 1.44$. Ceramic membranes, that have only recently become commercially available, should actually be better suited for such membrane reactor-separator applications.

Results and Discussion

Theoretical results

As evident in the theoretical model presented above, there are a number of parameters that affect the performance of the SLPCMRS. These are the permeabilities of species i in the various layers P_{i1}, P_{i2}, P_{iC}; the relative resistances of the membranes, Λ_1 to Λ_4; the diffusivity ratio, Ψ; the Thiele modulus, ϕ; the dimensionless flow rates, M_{AT}, M_{AS}, M_{BT}, and M_{BS}; and the liquid-loading in the catalyst layer, q. Of these parameters, the relative resistances of the membranes to the reactant and product, Λ_1 to Λ_4, play a crucial role in product separation. Usually, membrane 2 is selected such that it will give minimal resistance to the passage of both A and B through it, that is, $\Lambda_1, \Lambda_3 \gg \Lambda_2, \Lambda_4$, the primary objective of membrane 2 being to encapsulate the catalytic solution. The effective diffusion coefficients in the SLP layer, D_{AC} and D_{BC}, and hence the permeabilities of the SLP catalyst layer, P_{AC} and P_{BC}, depend on the liquid loading of the porous support disk (Eq. 6). If disk is completely filled with catalyst solution ($q = 1$), the effective diffusivity of A and B will be of the same order as the diffusivity in the catalyst solvent. On the other hand, if liquid loading is very low, then effective diffusivity will be considerably higher, being of the same order as the gas-phase diffusivity.

Figures 4 through 8 show the effect of the various variables on the performance of a differential SLPCMRS. The effect of the Thiele modulus on the reactant and product composition profiles in the membrane-catalyst composite is shown in Figure 4 in the absence of any substantial resistance to transport in the membranes, that is, Λ_1 to $\Lambda_4 = 1 \times 10^{-4}$, and at large values of the flow rates, F_T and F_S, so that $C_{AT}/C_T \to 1$, while C_{BT}/C_T, C_{AS}/C_T, and $C_{BS}/C_T \to 0$. The composition of A and B shown in the figure is made dimensionless with the *total* concentration of the reactant stream, C_T.

In Figures 5 and 6, the effect of varying the relative resistance of membrane 1 to the reactant (Λ_1) and to the product (Λ_3) on the composition profiles, respectively, is shown assuming the resistance of membrane 2 to be negligible. Λ_1 is varied between 0 and 1 in Figure 5. For reactant A, an increase of membrane 1 resistance decreases reactant concentration in the reaction

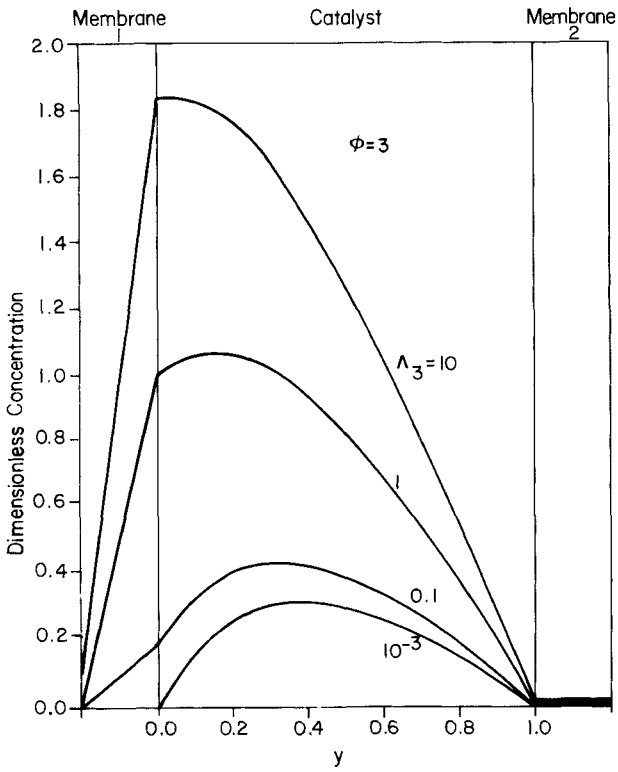

Figure 6. Effect of membrane 1 relative resistance (Λ_3) on the dimensionless product (*B*) concentration in the composite for $\phi = 3$ and negligible membrane relative resistances, $\Lambda_1 = \Lambda_2 = \Lambda_4 = 1 \times 10^{-4}$.

The dimensionless reactant and product cell flow rates are very high (M_{iT}, $M_{iS} \to \infty$) so that $C_{AT}/C_T \to 1$, while C_{BT}/C_T and $C_{BS}/C_T \to 0$.

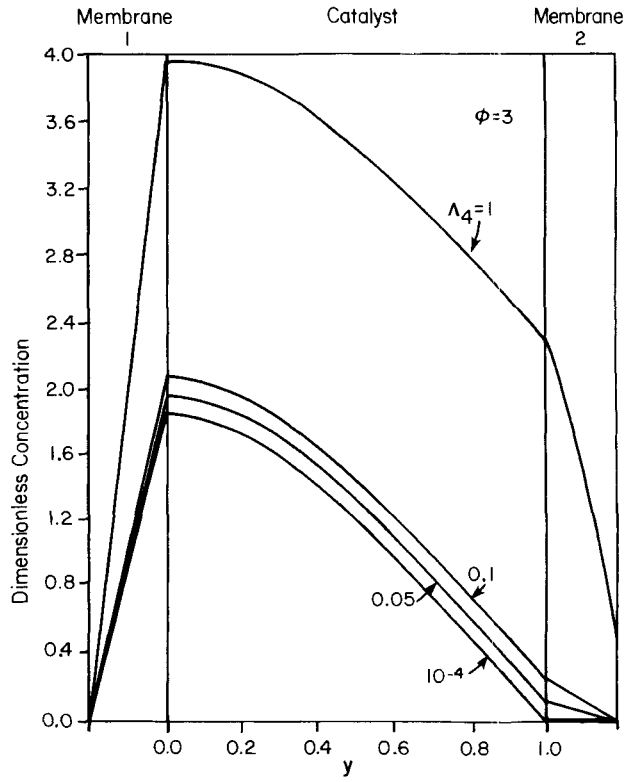

Figure 7. Effect of membrane 2 relative resistance (Λ_4) on the dimensionless product (*B*) concentration in the composite for $\phi = 3$ and the membrane relative resistances, $\Lambda_3 = 10$, and $\Lambda_1 = \Lambda_2 = 1 \times 10^{-4}$.

The dimensionless reactant and product cell flow rates are very high (M_{iT}, $M_{iS} \to \infty$) so that $C_{AT}/C_T \to 1$, while C_{BT}/C_T and $C_{BS}/C_T \to 0$.

zone, thereby decreasing the overall catalyst layer effectiveness. For product *B* (Figure 6), more product will accumulate at the interface of membrane 1 and catalyst layer as the membrane 1 relative resistance for *B* (Λ_3) increases and flux of the product at membrane 2 will increase directly with the increasing concentration gradient there, thus resulting in increased product recovery in the product cell. Therefore, the desirable traits for membrane 1 are that it should have a high permeability for the reactant but should offer a high resistance to the product. In other words, it ideally should possess high permselectivity.

In Figure 7, the effect of the resistance of membrane 2 (Λ_4) on product accumulation inside the reaction zone is shown for $\Lambda_1 = \Lambda_2 = 1 \times 10^{-4}$ and $\Lambda_3 = 10$. Since membrane 1 is already providing impediment to the product flux to the reactant cell, membrane 2 should have a minimum resistance toward the product flux to facilitate product recovery. For this reason, in the experimental study, microporous membrane with approximately 0.2-μm pore size was used. The effect of the dimensionless flow rate in the product cell, M_{BS}, on the composition profile is shown in Figure 8. As shown, the concentration gradient at the product stream increases with the sweep flow rate with a concomitant increase in the overall product recovery, although the product stream concentration reduces correspondingly.

The relative membrane 1 transport resistances to the reactant and the product, Λ_1 and Λ_3, depend on membrane 1 permeability, P_{i1}, and catalyst layer permeability, P_{iC}, and the latter depends on the liquid loading, q. Using typical values of the parameters, $P_{il} = 1 \times 10^{-3}$ cm/s, $D_{ije} = 1 \times 10^{-2}$ cm^2/s, and $D_{iL} = 1 \times 10^{-5}$ cm^2/s, the relative membrane resistances were calculated at various liquid loadings (Table 4). As q increases, more void volume is filled with solution, and the catalyst layer permeability decreases since diffusion through catalyst layer is controlled by liquid catalyst phase rather than by residual gas phase. At full loading ($q = 1$), the resistance of catalyst layer is much larger than the resistance of membrane and the product separation is low. When loading decreases, the relative membrane resistance increases with a sharp increase in product separation. This implies that at high catalyst loading a permselective membrane is required for efficient product separation. Of course, P_{iC} can also be increased by reducing the catalyst layer thickness, L_C, which could permit higher liquid loadings for situations where this is warranted for optimal performance.

Catalyst activity and stability

Catalytic activity and stability were first measured in the continuous-flow stirred-cell reactor using low liquid loading ($q = 5$ to 20%) of the catalyst disk. No membranes were used for these kinetic experiments, and the bottom side of the catalyst support disk was sealed off by a thin teflon disk. The composition of ethylene in the reaction mixture was kept at

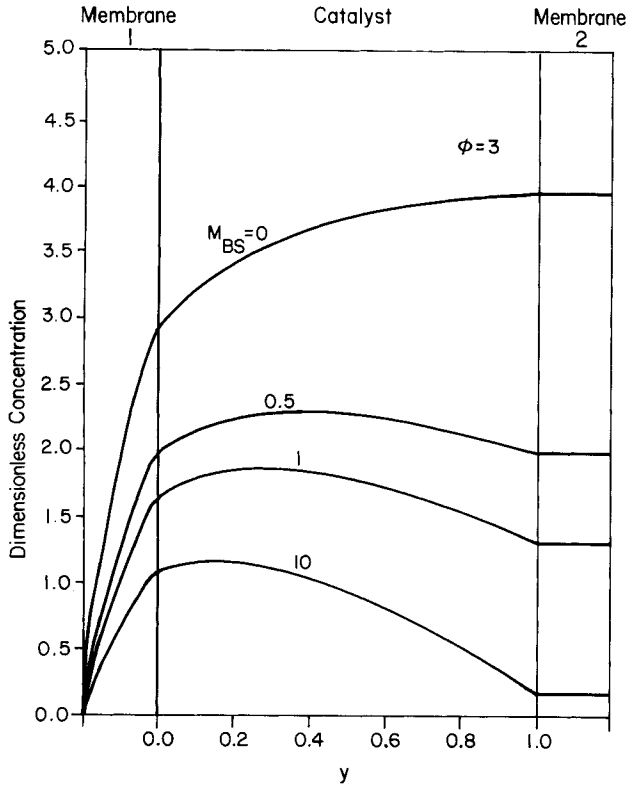

Figure 8. Effect of dimensionless sweep fluid flow rate (M_{BS}) on the dimensionless product (B) concentration in the composite for $\phi = 3$ and the membrane relative resistances, $\Lambda_3 = 1$, $\Lambda_1 = \Lambda_2 = \Lambda_4 = 1 \times 10^{-4}$, and $M_{iT} \to \infty$.

less than 10%, with CO and H_2 in excess, to ensure that the reaction rate is pseudo-first order with respect to ethylene concentration, C_{AC}, in the liquid phase. In terms of *gas*-phase concentration, C_{AT}, therefore,

$$-R_A = k K_{AC} C_{AT} \tag{36}$$

Material balance for ethylene yields:

$$F(C_{AO} - C_{AT}) = -R_A V_{\text{disk}} \epsilon q \eta \tag{37}$$

The effectiveness factor, η, for the SLPC layer for a first-order irreversible reaction is given by:

$$\eta = \frac{\tanh \phi_C}{\phi_C} \tag{38}$$

where the Thiele modulus is:

$$\phi_C \equiv L_C \sqrt{\frac{\epsilon q K_{AC} k}{D_{AC}}} \tag{39}$$

Assuming $\eta \to 1$ and $K_{AC} = 0.478$ (Rony and Roth, 1975), the pseudo-first-order rate constant was calculated as $k = 0.44\ s^{-1}$. To check the assumption of $\eta \to 1$, ϕ_C was calculated. For example, for $q = 0.05$, $\phi_C = 0.16$, and the corresponding $\eta = 0.992$. Hence, this supports the assumption of negligible diffusional resistance at low liquid loadings used for the kinetic experiments.

It was found that initially the catalyst activity decayed substantially over a period of a few hours before stabilizing. Since the ligand/catalyst ratio is a crucial factor in catalyst stability (Brown and Wilkinson, 1970), different runs were made at diffferent PPh_3/Rh mole ratios varying from about 15 to 50. It was found that catalyst solution with higher ligand concentration had relatively higher activity and was more stable. The other possible cause of catalyst deactivation is condensation of the aldehyde product inside the catalyst support pores. To confirm this, after one run the reactant flow into the reactor was stopped and reactor was heated for 1 hour at 80°C, while being purged with helium. The activity was found to increase again.

Table 4. Effect of Liquid Loading q on Relative Membrane Resistance Λ_3 and Separation*

Liquid Loading, q	Λ_3	Separation (%)
1.0	0.02	5.8
0.9	0.04	8.9
0.8	0.09	17.4
0.7	0.19	28.6
0.6	0.33	40.5
0.5	0.51	51.7
0.4	0.72	61.4
0.3	0.98	70.1
0.2	1.28	78.8
0.1	1.62	92.6

*$\phi_L = 30$, $\Lambda_2 = \Lambda_4 = 1 \times 10^{-4}$.

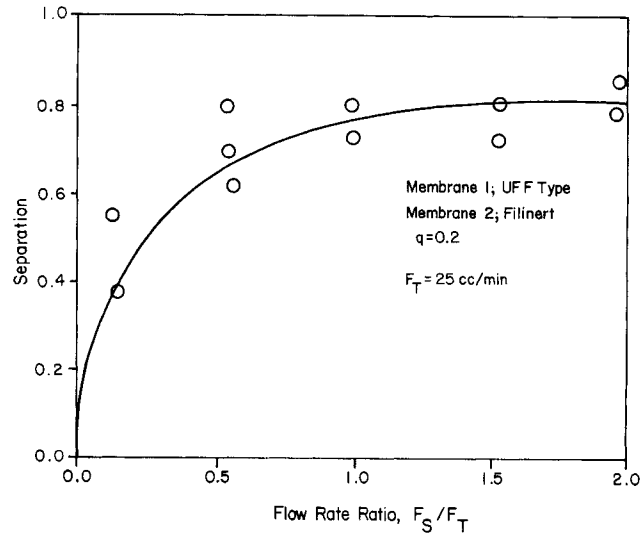

Figure 9. Experimental results and theoretical prediction of product separation (Eq. 34) as a function of the flow rate ratio, F_S/F_T.

SLPCMRS experiments

The pressure of the top compartment of the stirred cell reactor-separator was maintained at 65–75 psig (450–520 kPa) with continuous flow of reactants at 25 std. cm^3/min, while the bottom side was purged with helium flow at 20–40 psig

Table 5. Values of Parameters Used in Model Calculations for Ethylene Hydroformylation at 110°C

Parameter	Value
Membrane area	45.4 cm^2
Binary diffusivity, D_{ABe}	1.2×10^{-2} cm^2/s
Liquid-phase diffusivity, D_{AL}	2.5×10^{-5} cm^2/s
Rate constant, k	0.44 s^{-1}
Partition coefficient, K_{AC}	0.478
Flow rate ratio, F_S/F_T	0.5-2.0

(140-280 kPa). The purge stream flow rate was varied between 0-100 std. cm^3/min. Table 3 summarizes the conditions employed in the membrane composite experiments. The relative resistance of the membrane and catalyst layer was varied by controlling catalyst liquid loading of the porous support. Since the pore size of the catalyst support disk is much larger (90 μm) than that of the membranes, the resistance to transport in the catalyst layer is much smaller than that of the membrane layer when the catalyst loading is relatively low (<20%). In this case, the product formed in the catalyst zone is easily transported toward the product chamber resulting in substantial product recovery.

Experimentally, the extent of separation achieved was calculated by using measured flow rates of reactant and product streams, F_T and F_S, and the product concentration in each stream in the second part of Eq. 34. Figure 9 shows the experimental data with a liquid loading of 20% for product separation vs. the flow rate ratio, F_S/F_T, for a constant value of F_T=25 std. cm^3/min, while varying the sweep flow rate in the range 0-100 std. cm^3/min. All the data were obtained at a fixed time in each run after the catalyst activity had stabilized. Also plotted in Figure 9 is the theoretically predicted separation (Eq. 34 and Table 5). Overall, the experimental results agree quite well with the theoretical predictions. It is also seen that

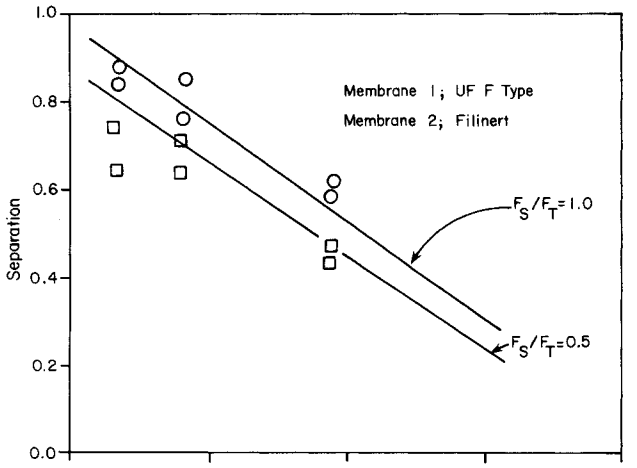

Figure 10. Experimental results and theoretical prediction of product separation (Eq. 34) as a function of the liquid loading, q, of the SLP catalyst layer.

The circles represent data for F_S/F_T=1.0, and squares represent data for F_S/F_T=0.5.

up to about 80% of the propionaldehyde produced is recovered on the product side. This provides conclusive evidence of the efficacy of the membrane reactor-separator for homogeneous catalysis described in this article in not only encapsulating the catalyst solution but also effectively separating the product from reactant.

In Figure 10, the separation obtained is plotted as a function of the liquid loading q of the SLP catalyst layer at two different flow rate ratios. At a catalyst loading of 20%, approximately 80% of the product was recovered in the product stream at the flow ratio of 1. As the catalyst loading increases, the product recovery is seen to drop substantially. The permeability of catalyst solution layer (P_{AC}, P_{BC}) decreases as q increases, and hence, the relative membrane resistance (Λ_3) also decreases. This causes the overall separation to decrease, as shown in Figure 10.

Conclusion

The proposed supported liquid-phase catalytic membrane reactor-separator for homogeneous catalysis, which is designed to encapsulate the liquid-phase catalyst solution and simultaneously accomplish product separation form reactant, was successfully demonstrated in this study by using the model reaction system of homogeneously catalyzed ethylene hydroformylation by $RhHCO(PPh_3)_3$ dissolved in dioctyl phthalate and supported to varying extents on a porous disk sandwiched between two different membranes. A theoretical model was developed to predict the performance of a stirred-cell membrane reactor-separator for a first-order reaction. The model agreed quite well with the experimental results. It was determined that for effective separation of the product, the transport resistance of the catalyst layer should be lower than that for the membranes. This is experimentally made possible in the proposed device by controlling the liquid loading of the supported liquid-phase catalyst layer.

The most difficult problem encountered in the experiments was the degradation of the membranes at the reaction conditions. With the recent advent of commercially available ceramic membranes, the SLPCMRS appears to hold potential for practical applications.

Acknowledgment

This work was supported by NSF grant number CPE-8217567. The suggestions made by Professor Sun-Tak Hwang, University of Cincinnati, are gratefully acknowledged.

Notation

a_1 = constant of integration, Eq. 22
a_2 = constant of integration, Eq. 23
A = area of membrane-catalyst composite; reactant (ethylene)
B = product (propionaldehyde)
C_{AO} = feed concentration of species A in the reactant cell
C_{AS} = concentration of species A in the product cell
C_{AT} = concentration of A in the reactant cell
C_{ig} = concentration of species i in region g
C_T = total concentration in the reactant cell
D_{i1} = effective diffusivity of i in membrane 1
D_{i2} = effective diffusivity of i in membrane 2
D_{iC} = effective diffusivity of i in the catalyst layer
D_{ije} = effective binary gas phase diffusivity if species i and j
D_{iL} = effective diffusivity of species i in the liquid phase
F_S = volumetric flow rate in the product cell

F_T = volumetric flow rate in the reactant cell
K_{i1} = partition coefficient if species i in membrane 1, C_{i1}/C_{iF}
K_{i2} = partition coefficient if species i in membrane 2, C_{i2}/C_{iF}
K_{iC} = partition coefficient if species i in catalyst layer, C_{iC}/C_{iF}
K_{iL} = partition coefficient if species i in liquid, C_{iL}/C_{iF}
L_1 = thickness of membrane 1
L_2 = thickness of membrane 2
L_C = thickness of catalyst layer
M_{AS} = dimensionless flow rate parameter, F_S/AP_{AC}
M_{AT} = dimensionless flow rate parameter, F_T/AP_{AC}
M_{BS} = dimensionless flow rate parameter, F_S/AP_{BC}
M_{BT} = dimensionless flow rate parameter, F_T/AP_{BC}
N_{iz} = flux of species i in the z-direction
P_{AC} = permeability of catalyst layer for species A, $D_{AC}\,K_{AC}/L_C$
P_{BC} = permeability of catalyst layer for species B, $D_{BC}\,K_{BC}/L_C$
P_{i1} = permeability of membrane 1 for species i, $D_{i1}\,K_{i1}/L_1$
P_{i2} = permeability of membrane 1 for species i, $D_{i2}\,K_{i2}/L_2$
P_{iC} = permeability of catalyst layer for species i, $D_{iC}\,K_{iC}/L_C$
P_S = total pressure in product cell
q = liquid catalyst loading, defined as the fraction of pore volume occupied by catalyst solution
R_i = rate of production of species i per unit volume of catalyst layer by reaction
T = temperature
V_{disk} = total volume of catalyst support disk
y = dimensionless distance into the catalyst layer, $(z-b)/L_C$
z = distance from the top in the catalyst-membrane composite

Greek letters

ϵ = porosity of catalyst support
ϕ = Thiele modulus for SLPC layer, Eq. 15
ϕ_C = Thiele modulus defined by Eq. 39
ϕ_L = Thiele modulus for completely liquid-filled support ($q=1$)
η = effectiveness factor for the catalyst layer
Λ_1 = relative membrane resistance or permeability ratio, P_{AC}/P_{A1}
Λ_2 = relative membrane resistance or permeability ratio, P_{AC}/P_{A2}
Λ_3 = relative membrane resistance or permeability ratio, P_{BC}/P_{B1}
Λ_4 = relative membrane resistance or permeability ratio, P_{BC}/P_{B2}
Ψ = diffusivity ratio of A and B in the catalyst layer, D_{AC}/D_{BC}

Subscripts

1 = membrane 1
2 = membrane 2
A = reactant (ethylene)
B = product (propionaldehyde)
C = catalyst layer
F = fluid phase (region T or S)
g = region g
i = species i
L = liquid phase
O = inlet to reactant cell
S = product cell
T = reactant cell

Literature Cited

Brown, C. K., and G. Wilkinson, "Homogeneous Hydroformylation of Alkenes with Hydridocarbonyltris (Triphenylphosphine) Rhodium(I) as Catalyst," *J. Chem. Soc.* (*A*), 2753 (1970).

Cheryan, M., *Ultrafiltration Handbook*, Technomic Pub. Co., Lancaster, PA (1986).

Cheryan, M., and M. A. Mehaia, "Membrane Bioreactors," *CHEMTECH*, 676 (Nov., 1986).

Cornils, B., *New Synthesis with Carbon Monoxide*, J. Falbe, ed., Springer Verlag (1980).

Datta, R., and R. G. Rinker, "Supported Liquid-Phase Catalysis: I. a Theoretical Model for Transport and Reaction," *J. Catal.*, **95**, 181 (1985).

Datta, R., J. Rydant, and R. G. Rinker, "Supported Liquid-Phase Catalysis: III. Experimental Evaluation of Diffusion-Reaction Model," *J. Catal.*, **95**, 202 (1985).

Davis, J. C., "Kinetics Studies in a Continuous Steady State Hollow Fiber Membrane Enzyme Reactor," *Biotechnol. Bioeng.*, **16**, 1113 (1974).

Davis, R. J., J. A. Rossin, and M. E. Davis, "Hydroformylation by Rhodium Zeolite A Catalysts," *J. Catal.*, **98**, 477 (1986).

Gosser, L. W., W. H. Knoth, and G. W. Parshall, "Reverse Osmosis in Organometallic Synthesis," *J. Amer. Chem. Soc.*, **95**, 3436 (1973).

Gosser, L. W., W. H. Knoth, and G. W. Parshall, "Reverse Osmosis in Homogeneous Catalysis," *J. Mol. Catal.*, **2**, 253 (1977).

Haggin, J., "Membranes Play Growing Role in Small-Scale Industrial Processing," *C&EN*, 25 (July, 1988).

Hartley, F. R., *Supported Metal Complexes*, D. Reidel Pub. Co., Dordrecht, Holland (1985).

Hong, J., G. T. Tsao, and D. C. Wankat, "Membrane Reactor for Enzymatic Hydrolysis of Cellobiose," *Biotechnol. Bioeng.*, **23**, 1501 (1981).

Itoh, N., "A Membrane Reactor Using Palladium," *AIChE J.*, **33**, 1576 (1987).

Jennings, J. F., and R. C. Binning, U.S. Patent No. 2,956,070 (1960).

Kim, J. S., and R. Datta, "Membrane Reactor-Separator for Homogeneous Catalysis," AIChE Meeting, New York (1987).

Matson, S. L., and J. A. Quinn, "Membrane Reactors in Bioprocessing," *Ann. N.Y. Acad. Sci.*, **469**, 152 (1986).

Murrell, L. L., "Immobilization of Transition Metals: Complex Catalysts on Inorganic Supports," *Advanced Materials in Catalysis*, J. J. Burton and R. L. Garten, eds., Academic Press, New York (1977).

Oliver, K. L., and F. B. Booth, "A New Process for the Hydroformylation of Olefins," *ACS, Div. of Pet. Chem.*, Preprints, **14**(3), A7 (1969).

Ollis, D. F., J. B. Thompson, and E. T. Wolynic, "Catalytic Liquid Membrane Reactor: I. Concept and Preliminary Experiments in Acetaldehyde Synthesis," *AIChE J.*, **18**, 457 (1972).

Parshall, G. W., "Industrial Applications of Homogeneous Catalysis: a Review," *J. Mol. Catal.*, **4**, 243 (1978).

Parshall, G. W., *Homogeneous Catalysis: The Applications and Chemistry of Catalysis by Soluble Transition Metal Complexes*, Wiley, New York (1981).

Parshall, G. W., and R. E. Putscher, "Organometallic Chemistry and Catalysis in Industry," *J. Chem. Edu.*, **63**, 189 (1986).

Pittman, C. U., "Polymer Supported Catalysts," *Comprehensive Organometallic Chemistry*, Vol. 8, p. 553, G. Wilkinson, F. G. A. Stone, and E. W. Abel, eds., Pergamon Press, Oxford (1982).

Rao, V., and R. Datta, "Development of a Supported Molten-Salt Wacker Catalyst for the Oxidation of Ethylene to Acetaldehyde," *J. Catal.*, **114**, 377 (1988).

Rony, P. R., "Supported Liquid-Phase Catalysts," *Chem. Eng. Sci.*, **23**, 1021 (1968).

Rony, P. R., "Multiphase Catalysis. II. Hollow Fiber Catalysts," *Biotechnol. Bioeng.*, **13**, 431 (1971).

Rony, P. R., "Hollow Fiber Enzyme Reactors," *J. Amer. Chem. Soc.*, **94**, 8247 (1972).

Rony, P. R., and J. F. Roth, "Supported Metal Complex Catalysts," *J. Mol. Catal.*, **1**, 13 (1975).

Shinji, O., M. Misono, and Y. Yonedo, "Dehydrogenation of Cyclohexane by Use of a Porous Glass Reactor," *Bull. Chem. Soc. Japan*, **55**, 2760 (1982).

Sun, Y-M., and S-J. Khang, "Catalytic Membrane for Simultaneous Chemical Reaction and Separation Applied to a Dehydrogenation Reaction," *Ind. Eng. Chem. Res.*, **27**, 1136 (1988).

Vick Roy, T. B., H. W. Blanch, and C. R. Wilke, "Lactic Acid Production by *Lactobacillus Delbreuckii* in a Hollow Fiber Fermenter," *Biotechnol. Lett.*, **4**, 483 (1982).

Wang, D. I. C., A. J. Sinskey, and T. A. Butterworth, *Membrane Science and Technology*, J. E. Flinn, ed., Plenum, New York (1970).

Manuscript received July 18, 1991, and revision received Sept. 25, 1991.